Momentum kick model analysis of PHENIX near-side ridge data and photon jet

Cheuk-Yin Wong (黃卓然)*
Physics Division, Oak Ridge National Laboratory, Oak Ridge, Tennessee 37831, USA
(Received 7 January 2009; revised manuscript received 20 July 2009; published 28 September 2009)

We analyze PHENIX near-side ridge data for central Au + Au collisions at $\sqrt{s_{NN}} = 200$ GeV with the momentum-kick model, in which a near-side jet emerges near the surface, kicks medium partons, loses energy, and fragments into the trigger particle and fragmentation products. The kicked medium partons subsequently materialize as the observed ridge particles, which carry direct information on the early parton momentum distribution and the magnitude of the momentum kick. We find that the PHENIX ridge data can be described well by the momentum-kick model and the extracted early partons momentum distribution has a thermal-like transverse distribution and a rapidity plateau structure. We also find that the parton-parton scattering between the jet parton and the medium parton involves the exchange of a nonperturbative pomeron, for jet partons in momentum range considered in the near-side ridge measurements.

DOI: 10.1103/PhysRevC.80.034908 PACS number(s): 25.75.Gz, 25.75.Dw

I. INTRODUCTION

Recently, the STAR Collaboration [1–13] observed a $\Delta\phi$-$\Delta\eta$ correlation of particles associated with a high-p_t near-side hadron trigger particle in central Au + Au collisions at $\sqrt{s_{NN}} = 200$ GeV, where $\Delta\phi$ and $\Delta\eta$ are the azimuthal angle and pseudorapidity differences measured relative to the trigger particle, respectively. Particles associated with the near-side jet can be decomposed into a "jet component" at $(\Delta\phi, \Delta\eta) \sim (0,0)$ and a "ridge component" at $\Delta\phi \sim 0$ with a ridge structure in $\Delta\eta$. A similar correlation with a high-p_t trigger has also been observed by the PHENIX Collaboration [14–16] and the PHOBOS Collaboration [17]. Recent reviews of the ridge phenomenon have also been presented [18–20].

In this article, we shall limit our attention to the ridge phenomenon involving a high-p_t jet on the near side. We shall not consider ridge-type $\Delta\phi$-$\Delta\eta$ correlations that have also been observed between two low-p_t hadrons [21], as they do not involve the occurrence of a high-p_t jet on the near side.

Many theoretical models [22–43] have been proposed to discuss the ridge phenomenon. The model of Ref. [27] assumes that the ridge particles arise from the extra particles deposited by the forward and backward beam jets at the source point associated with the two transverse jets. The correlation of the jet source transverse position and the transverse medium flow then leads to an azimuthal distribution with a width in $\Delta\phi$ [27,28]. The width in $\Delta\phi$ obtained from such a model is wide in comparison with experimental data [27]. The correlated emission model [29–32] assumes that ridge particles arise from soft thermal gluons radiated along the jet direction, with an enhancement due to the radial flow. The models of Refs. [27] and [29] deal with the azimuthal correlations in the central rapidity region, and the pseudorapidity correlation has not yet been considered. The backsplash model assumes that the ridge on the near-side arises from the hydrodynamical backsplash of the away-side jet flow [33]; hydrodynamical calculations for such a model has not yet been made. The Glasma model examines $\Delta\phi$-$\Delta\eta$ correlation between two low-p_t hadrons [21] without a high-p_t trigger and assumes that the ridge in soft low-p_t pairs arises from the initially boost-invariant distribution that persists in the bulk matter for low-p_t particles [34–36]. The jet broadening models [37–40] consider the ridge particles as arising from radiated gluons of the incident jet; they have not been compared quantitatively with the ridge data. Taking the features of jet broadening as free parameters in a hydrodynamical calculation leads to a theoretical jet peak to ridge ratio large in comparison with experiment [41]. The possibility of the intermediate p_t trigger arising from the medium-medium recombination adds further complications to the analysis of the ridge phenomenon [42,43]. The recent PHOBOS observation that the ridge extends to pseudorapidity separations as large as $|\Delta\eta| \sim 4$ [17] provides an important test for the models.

Successful analyses of experimental near-side data have been obtained in the momentum-kick model, over large phase space of the associated particles in p_t, $\Delta\phi$, and $\Delta\eta$ [22–25]. In this model, the ridge particles are described as arising from partons in the medium that are kicked by the jet. We envisage that a near-side jet emerges near the surface, kicks (or scatters) medium partons, loses energy, and fragments into the trigger particle and fragmentation products. By assumption of parton-hadron duality, the kicked (or scattered) medium partons subsequently materialize as the observed ridge particles, which can be used to extract valuable information on the jet-medium interaction and the properties of the early parton medium. In the description of the interaction between the medium and a jet in the momentum-kick model, we have chosen to represent the medium as particles instead of fields, because of (i) the short-range nature of the color screening interaction between partons in a dense color medium [44,45] and (ii) the observed azimuthal kinematic correlation between the ridge particles and the trigger jet.

Our task can be made easier here as we can divide the theoretical analysis in three steps. The first step is to set up the basic phenomenological theory of the momentum-kick model in which physical quantities enter as important parameters. The second step consists of comparing the extracted physical

*wongc@ornl.gov

quantities with those in other observed phenomena. The third step consists of constructing fundamental theoretical models that can explain these physical quantities.

Following such a strategy, we describe the production process of associated particles as consisting of the jet component and the ridge component. The ridge component depends on the magnitude of the momentum kick, the number of jet-(medium parton) collisions, and the shape of the early medium parton momentum distribution. However, the jet component yield per trigger in a nucleus-nucleus collision can be described as an attenuated jet component of a pp collision. It is therefore necessary to analyze the auxiliary associated particle yield in pp collisions to specify the jet component in nucleus-nucleus collisions.

Our successful description of the experimental data allows us to extract physical quantities from STAR near-side ridge data in central Au + Au collisions at $\sqrt{s_{NN}} = 200$ GeV [25]. In the process, we infer that the shape of the early parton momentum distribution possesses a thermal-like transverse distribution and a rapidity plateau structure. We find that the magnitude of the longitudinal momentum kick is about 1 GeV per jet-(medium parton) collision. We infer also that for a central Au + Au collision the number of jet-(medium parton) collision multiplied by the attenuation factor is about 4. As not much is known about these physical quantities, the extracted quantities provide useful insight into the properties of the early partons and their interactions with the jet in nucleus-nucleus collisions.

With the successes in analyzing the STAR near-side ridge data, it is of interest to see whether the momentum-kick model is consistent with other experimental measurements. Our first test of the momentum-kick model gives a good prediction [24,25] of the PHOBOS data [17] at large rapidities, indicating the approximate validity of the momentum-kick model and the presence of the rapidity plateau.

We wish to analyze here the PHENIX ridge data that cover a smaller region of pseudorapidities, $|\eta^{\rm trig}, \eta^{\rm assoc}| < 0.35$ but a large number of $p_t^{\rm trig} \otimes p_t^{\rm assoc}$ combinations. Both the jet and ridge components contribute and interplay in the small $\Delta\eta$ region on the near side of the jet. This is different from the STAR and PHOBOS ridge data that cover a large range of pseudorapidities. The jet component is important at $\Delta\eta \sim 0$, whereas the ridge component dominates for $|\Delta\eta| > 0.7$.

After extracting the physical quantities from the analysis of the PHENIX ridge data, we wish to find out the nature of the scattering between the jet parton and the medium parton. In the experimental setup, jet triggers have been accepted in the interval $2 < p_t^{\rm trig} < 10$ GeV. The incident jet parton has an initial transverse momentum of order $p_t^{\rm jet} \sim 10$ GeV, as a jet parton loses a few GeV in kicking a few medium partons. Is the scattering between a jet parton and a medium parton a perturbative or nonperturbative QCD scattering process, for jet partons in this momentum range? Our ability to ascertain the nature of the parton-parton scattering will help us select the proper description to formulate the process of energy loss for these jet partons.

Previously, phenomenological model of hadron-hadron differential cross section in terms of parton-parton collisions with a finite correlation length was successfully applied in the modified Chou-Yang model [46–49]. In recent years, much progress has been made on the description of nonperturbative parton-parton scattering, in connection with a better understanding on the nature of the nonperturbative soft pomeron [50–60]. In particular, hadron-hadron elastic differential cross section analysis and lattice gauge calculations support the concept of the structure of a pomeron with a small correlation length. These recent theoretical advances will allow us to compare the characteristics of the parton-parton scattering in the present momentum-kick model with those parton-parton collisions arising from the exchange of nonperturbative pomerons.

Turning to the properties of the early parton momentum distribution extracted from the momentum-kick model, we note that the presence of the rapidity plateau in the early history of a central nucleus-nucleus collision as inferred from the momentum-kick model is not a surprising result, as the rapidity plateau structure occurs in elementary processes involving the fragmentation of flux tubes [26,61–64] and in many particle production models such as models based on preconfinement [65], parton-hadron duality [66] cluster fragmentation [67], string-fragmentation [68], dual-partons [69], the Venus model [70], the Relativistic quantum molecular dynamics (RQMD) model [71], multiple collision model [72], parton cascade model [73,74], color-glass condensate model [75], a multi-phase transport (AMPT) model [76], the Lexus model [77], and many others. To investigate the origin of the rapidity plateau in a quantum mechanical framework, we can go a step further to use the physical argument of transverse confinement to establish a connection between QCD and QED2 (quantum electrodynamics in 2 dimensions) [25,26]. One finds that a rapidity plateau of produced particles is a natural occurrence when color charges pull away from each other at high energies [26,61–64] as in QED2 [78–81]. Experimental evidence for a rapidity plateau along the sphericity axis or the thrust axis has been observed earlier in $\pi^{\pm}$ production in high-energy e^+-e^- annihilations [82–86]. A rapidity plateau structure has also been observed in pp collisions at RHIC energies by the BRAHMS Collaboration [87].

In addition to the magnitude of the momentum kick acquired by a medium parton per jet (medium parton) collision, the ridge data also give information on the number of kicked partons. These physical quantities are clearly related to the energy loss of a jet in the dense medium. A consistent picture of both the ridge yield and jet quenching emerges from the momentum-kick model analyses [25] and complements other studies of the jet quenching phenomenon [88].

The analysis of the PHENIX near-side ridge data also provides an opportunity to examine an additional test of the momentum-kick model using a high-p_t photon jet. Nucleon-nucleon collisions can lead to the occurrence of a high-p_t parton jet in coincidence with a high-p_t photon jet. In a central nucleus-nucleus collision with an away-side parton jet, we can use a photon jet on the near-side to test different ridge models [89]. By comparing associated particles on the near-side with a hadron or a photon jet, we can separate out effects owing to the collision of the near-side jet. If the ridge arises from the medium as a result of the collision of the near-side parton jet, as in the momentum-kick model, the substitution of a near-side photon jet will lead to a greatly reduced yield of

ridge particles. If the ridge particles arise from "several extra particles deposited by forward-backward beam jets into the fireball," as in the position-flow model of Refs. [27] and [28] then the near-side ridge will remain for a near-side photon jet. If the ridge arises from the backsplash of the propagation of away-side parton jet, then the large ridge structure will remain for a near-side photon jet. It is therefore of interest to make theoretical estimates of the ridge yield in association with a near-side, high-p_t photon jet in the momentum-kick model so as to assist experiments in such an analysis.

This article is organized as follows. In Sec. II, we review and summarize the main results of the momentum-kick model. In Sec. III, we discuss the jet component in Au + Au and in pp collisions. The auxiliary associated particles yield in pp collisions is parametrized to assist the analysis of the ridge component in Au + Au collisions. In Sec. IV, momentum-kick model description of the ridge yield is presented and physical parameters are introduced to describe the ridge component. In Sec. V, we compare theoretical and experimental results of the total associated particle yield in PHENIX experiments using hadron triggers in different $p_t^{\rm trig}$ intervals. In Secs. VI, VII, and VIII, we examine new insights derived from the physical quantities extracted from the momentum-kick model. Specifically, in Sec. VI, we find that the magnitude of the longitudinal momentum kick along the jet direction q_L is consistent with the characterization that the scattering between the jet parton and the medium parton involves the exchange of a nonperturbative pomeron. In Sec. VII, we find that the extracted shape of the rapidity plateau of the early parton distribution is in between those of the pp and Au + Au collisions, indicating an intermediate stage of parton evolution. In Sec. VIII, we find that the number of kicked partons at the most central collision can provide the correct normalization for the momentum-kick model to describe the centrality dependence of the ridge yield. These results supports the approximate validity of the momentum-kick model. In Sec. IX, we calculate the ridge yield when a high-p_t photon jet occurs. The results can be used to guide our search for ways to discriminate different models. In Sec. X, we present our discussions and conclusions.

II. REVIEW OF THE MOMENTUM-KICK MODEL

We shall briefly summarize the basic concepts of the momentum-kick model. In the phenomenon of the ridge associated with the near-side jet, it is observed that (i) the ridge particle yield increases with the number of participants, (ii) the ridge yield appears to be nearly independent of the trigger jet properties, (iii) the baryon to meson ratios of the ridge particles are more similar to those of the bulk matter than those of the jet, and (iv) the slope parameter of the transverse distribution of ridge particles is intermediate between those of the jet and the bulk matter [1–20]. These features suggest that the ridge particles are medium partons, at an early stage of the medium evolution during the passage of the jet. The azimuthal correlation of the ridge particle with the jet and the presence of strong screening suggest that the associated ridge particle and the trigger jet are related by collisions. A momentum-kick model was put forth to explain the ridge phenomenon [22–26].

The model assumes that a near-side jet occurs near the surface, collides with medium partons, loses energy along its way, and fragments into the trigger and its associated fragmentation products (the "jet component"). Those medium partons that collide with the jet acquire a momentum kick along the jet direction. They subsequently materialize by parton-hadron duality as ridge particles in the "ridge component." In other words, the ridge particles are medium partons kicked by the jet and they carry direct information on the early parton momentum distribution and the magnitude of the longitudinal momentum kick.

As described in detail in Refs. [22–25], we follow a jet as it collides with medium partons in a dense medium and study the yield of associated particles for a given $p_t^{\rm trig}$. The evaluation of the ridge yield and the investigation of the quenching of the jet will be greatly simplified by using average values of various physical quantities, whose "average" attribute will be made implicit.

We label the normalized initial momentum distribution of medium partons at the moment of jet-(medium parton) collisions by $E_i dF/d\mathbf{p}_i$. The jet imparts a momentum $\mathbf{q}$ onto a kicked medium parton, which changes its momentum from $\mathbf{p}_i$ to $\mathbf{p} = (p_t, \eta, \phi) = \mathbf{p}_f = \mathbf{p}_i + \mathbf{q}$, as a result of the jet-(medium parton) collision. By assumption of parton-hadron duality, the kicked medium partons subsequently materialize as observed associated ridge particles.

We shall use the label $\mathbf{p}$ of the kicked medium partons interchangeably with the label $\mathbf{p}^{\rm assoc}$ of associated ridge particles. The normalized final parton momentum distribution $EdF/d\mathbf{p}$ at $\mathbf{p}$ is related to the normalized initial parton momentum distribution $E_i dF/d\mathbf{p}_i$ at $\mathbf{p}_i$ at a shifted momentum, $\mathbf{p}_i = \mathbf{p} - \mathbf{q}$, and we have [22]

$$\frac{dF}{p_t dp_t d\eta d\phi} = \left[\frac{dF}{p_{ti} dp_{ti} dy_i d\phi_i}\frac{E}{E_i}\right]_{\mathbf{p}_i=\mathbf{p}-\mathbf{q}} \times \sqrt{1 - \frac{m^2}{(m^2 + p_t^2)\cosh^2 y}}, \quad (1)$$

where the factor E/E_i ensures conservation of particle numbers and the last factor changes the rapidity distribution of the kicked partons to the pseudorapidity distribution [64].

We characterize the number of partons kicked by the jet by $\langle N_k \rangle$, which depends on the centrality and the jet-(medium parton) cross section. The (charged) ridge particle momentum distribution in a central $A + A$ collision per trigger is then

$$\begin{aligned}\left[\frac{dN_{\rm ch}}{N_{\rm trig} p_t dp_t d\Delta\eta\, d\Delta\phi}\right]^{AA}_{\rm ridge} &= \left[f_R \frac{2}{3}\langle N_k\rangle \frac{dF}{p_t dp_t\, d\Delta\eta d\Delta\phi}\right]^{AA}_{\rm ridge} \\ &= f_R \frac{2}{3}\langle N_k\rangle \left[\frac{dF}{p_{ti} dp_{ti} dy_i d\phi_i}\frac{E}{E_i}\right]_{\mathbf{p}_i=\mathbf{p}-\mathbf{q}} \\ &\quad \times \sqrt{1 - \frac{m^2}{(m^2 + p_t^2)\cosh^2 y}}, \end{aligned} \quad (2)$$

TABLE I. Physical parameters in Eq. (4), for the description of associated particles in pp collisions and the meaning of each parameter.

Category	Physical parameter	Meaning
Properties of jet particles associated with a trigger in a pp collision	$N_{\rm jet}$	Number of associated particles per trigger in a pp collision
	$T_{\rm jet}$	"Temperature" of $p_t^{\rm assoc}$ distribution in a pp collision
	$\sigma_{\phi 0}$	Jet cone width parameter
	m_a	Mass parameter to modify the variation of jet cone width σ_ϕ with $p_t^{\rm assoc}$

where $\Delta\eta = \eta - \eta^{\rm trig}$, $\Delta\phi = \phi - \phi^{\rm trig}$, f_R is the average survival factor for produced ridge particles to reach the detector, and the factor $2/3$ is to indicate that $2/3$ of the produced associated particles (presumably pions) are charged.[1] Present measurements furnish information only on the product $f_R\langle N_k\rangle$. The momentum kick $\mathbf{q}$ will be distributed in the form of a cone around the trigger jet direction with an average $\langle\mathbf{q}\rangle = q_L\,\mathbf{e}^{\rm trig}$ directed along the trigger direction $\mathbf{e}^{\rm trig}$, characterized by the momentum-kick magnitude q_L. For brevity of nomenclature, 'the longitudinal momentum kick q_L along the jet direction' will henceforth be abbreviatingly called 'the momentum kick q_L.'

III. THE JET COMPONENT IN Au + Au AND *pp* COLLISIONS

Experimental measurements of the associated particles in $A + A$ collisions include contributions from both the jet component and the ridge component. By comparing the associated particle yield per trigger in central Au + Au collisions with the pp associated particle yield at $\Delta\eta \sim 0$, one finds that in the region of $p_t < 4$ GeV, the jet component yield in central Au + Au collisions can be consistently described as an attenuated yield of associated particles in a pp collision [25],

$$\left[\frac{1}{N_{\rm trig}}\frac{dN_{\rm ch}}{p_t dp_t d\Delta\eta d\Delta\phi}\right]^{AA}_{\rm jet} = f_J\,\frac{dN^{pp}_{\rm jet}}{p_t dp_t d\Delta\eta d\Delta\phi}. \quad (3)$$

The survival factor f_J varies with $p_t^{\rm assoc}$ of the associated particles, being relatively constant for low $p_t^{\rm assoc}$ with a semiempirical value of $f_J = 0.632$ [25]. It reaches the value of unity when $p_t^{\rm assoc}$ of the associated particle approaches $p_t^{\rm trig}$, corresponding to fragmentation outside the medium [see the dependence of f_J on $p_t^{\rm assoc}$ in Eq. (15) below].

To obtain the jet component in Au + Au collisions, we need the yield of associated particles in a pp collision. In principle, the yield of associated particles can be obtained from the description of jets in perturbative QCD such as the PYTHIA computer program [90,91]. The application of such a treatment with different available sets of tuned parameters does not automatically yield a perfect agreement of the theory with experiment. Additional fine tuning of many PYTHIA parameters and theoretical options is needed [91]. Even with the fine-tuning, the agreement of theoretical results with both the experimental jet spectra and the experimental associated particle correlation cannot be obtained simultaneously at the present time [91].

For our purposes of studying the ridge phenomenon, the pp associate particle data are only auxiliary quantities that are needed to calculate the total associated particle yield. One could in principle make use of the experimental pp data to infer the jet component of the Au + Au jet component, with the help of Eq. (3). We shall alternatively represent the experimental pp data by simple parametrization, which is just a short-hand way to stand for the experimental pp associated particle data, for the purpose of assisting later the evaluation of the total associated particle yield.

The experimental associated particle distribution in pp collisions can be described well by [25]

$$\frac{dN^{pp}_{\rm jet}}{p_t dp_t d\Delta\eta d\Delta\phi} = N_{\rm jet}\frac{\exp\left\{\left(m - \sqrt{m^2 + p_t^2}\right)/T_{\rm jet}\right\}}{T_{\rm jet}(m + T_{\rm jet})} \times \frac{1}{2\pi\sigma_\phi^2}e^{-[(\Delta\phi)^2+(\Delta\eta)^2]/2\sigma_\phi^2}, \quad (4)$$

where by assumption of hadron-parton duality m is taken as the pion mass m_π, $N_{\rm jet}$ is the total number of near-side (charged) associated particles in a pp collision, and $T_{\rm jet}$ is the jet inverse slope ("temperature") parameter of the "pp jet component." In our search for parameter values we find that the parameters $N_{\rm jet}$ and $T_{\rm jet}$ vary linearly with $p_t^{\rm trig}$ of the trigger particle which we describe as[2]

$$N_{\rm jet} = N_{\rm jet0} + d_N\,p_t^{\rm trig}, \quad (5)$$

$$T_{\rm jet} = T_{\rm jet0} + d_T\,p_t^{\rm trig}. \quad (6)$$

We also find that the width parameter σ_ϕ depends slightly on p_t which we parametrize as

$$\sigma_\phi = \sigma_{\phi 0}\frac{m_a}{\sqrt{m_a^2 + p_t^2}}. \quad (7)$$

We summarize the meaning of the parameters introduced to describe the pp associated particle data in Table I.

Using this set of parameters, we fit the pp associated particle data obtained in PHENIX measurements for pp collisions at $\sqrt{s_{NN}} = 200$ GeV. The values of the parameters are given in

[1] The charge fraction (2/3) assumed for a pion system can be modified for a medium with a more general composition.

[2] In calculating the $N_{\rm jet}$ and $T_{\rm jet}$ parameters using Eqs. (5) and (6) for the interval of $p_t^{\rm trig} = 5$–10 GeV, we use $\langle p_t^{\rm trig}\rangle = 5.5$ GeV for this interval as the spectra of trigger particles decrease rapidly with $p_t^{\rm trig}$ and the dominant contributions for this interval come between $p_t^{\rm trig} = 5$ and 6 GeV.

TABLE II. Jet component parameters in Eq. (4) for associated particles with different $p_t^{\rm trig}$ triggers in pp collisions at $\sqrt{s_{NN}} = 200$ GeV.

Hadron trigger	$p_t^{\rm trig}$	STAR 4–6 GeV	PHENIX 2–3 GeV	PHENIX 3–4 GeV	PHENIX 4–5 GeV	PHENIX 5–10 GeV
Properties of particles associated with a trigger in pp collisions	$N_{\rm jet}$	0.75	$0.15 + 0.10\langle p_t^{\rm trig}\rangle$ GeV			
	$T_{\rm jet}$	0.55 GeV	0.19 GeV + $0.06\langle p_t^{\rm trig}\rangle$			
	$\sigma_{\phi 0}$		0.50			
	m_a		1.1 GeV			

Table II. The theoretical results of $dN_{\rm ch}^{pp}/N_{\rm trig}\, d\Delta\phi$ are given as dash-dot curves in Fig. 1 and the corresponding experimental data are represented by open circles. As one observes in Fig. 1, although the fit is not perfect, the set parameters in Table II adequately describe the set of pp associated particle data for $2 < p_t^{\rm trig} < 10$ GeV and for $0.4 < p_t^{\rm assoc} < 4$ GeV. The parametrization can be used to generate the jet component for nucleus-nucleus collisions by assuming that the jet component yield per trigger in a nucleus-nucleus collision is an attenuated yield of the corresponding pp collision.

As indicated in Table II, the parameters of Eqs. (5) and (6) are $N_{\rm jet0} = 0.15$, $d_N = 0.1$/GeV, $T_{\rm jet0} = 0.19$ GeV, and $d_T = 0.06$. Thus, particles associated with the pp collisions changes its properties significantly as $p_t^{\rm trig}$ changes.

We can compare the parameters obtained here with those from our previous analysis of the STAR near-side ridge data for central (0–5%) Au + Au collisions at $\sqrt{s_{NN}} = 200$ GeV with $4 < p_t^{\rm trig} < 6$ GeV. The associated particles in pp collisions in the STAR measurements can be described by Eq. (4) with parameters [25]

$$N_{\rm jet} = 0.67, \quad T_{\rm jet} = 0.55 \text{ GeV}, \\ \sigma_{\phi 0} = 0.50 \text{ GeV}, \quad \text{and} \quad m_a = 1.1 \text{ GeV}, \tag{8}$$

as shown in column 3 of Table II. They are consistent with those for the PHENIX-associated particle data in pp collisions.

IV. TOTAL YIELD OF ASSOCIATED PARTICLES

The total observed yield of associated particles per trigger in $A + A$ collisions consists of the sum of the jet and the ridge

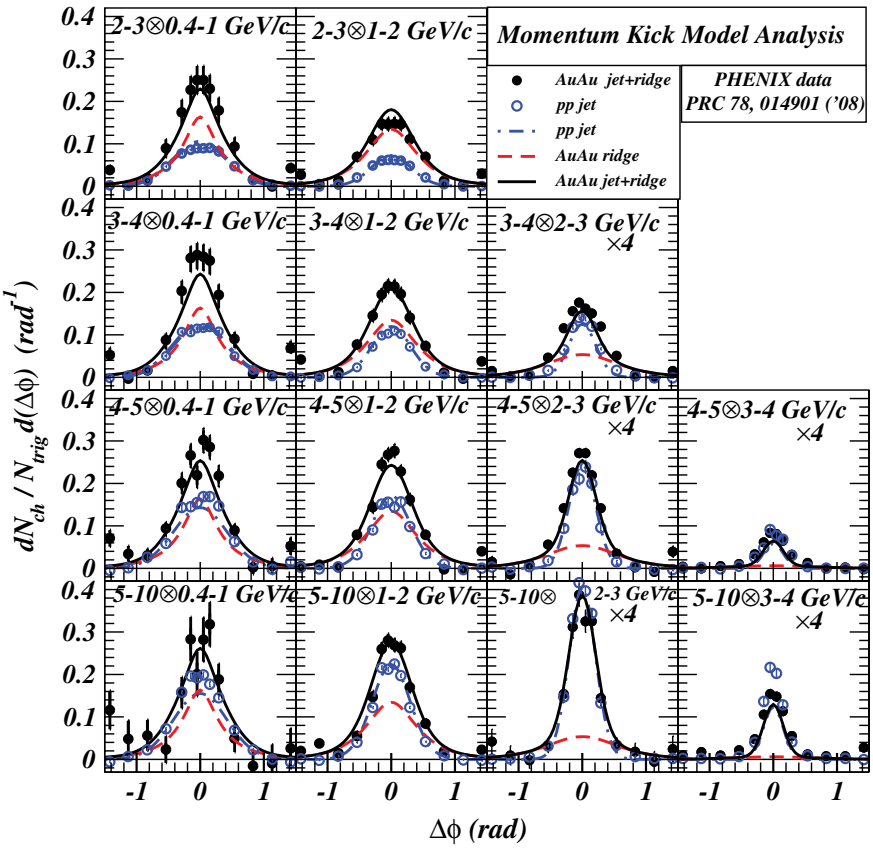

FIG. 1. (Color online) PHENIX azimuthal angular distribution of associated particles per trigger in different $p_t^{\rm trig} \otimes p_t^{\rm assoc}$ combinations. The solid and open circles are the total associated particle yield per trigger, $dN_{\rm ch}/N_{\rm trig}\, d\Delta\phi$, in central Au + Au and pp collisions, respectively [14]. The solid, dashed, and dashed-dot curves are the theoretical total Au + Au associated particle yields per trigger, the Au + Au ridge particle yields per trigger, and the pp associated particle yields, respectively.

TABLE III. Physical parameters in Eqs. (2), (3), and (10) in the momentum-kick model and the meaning of each parameter.

Category	Physical parameter	Meaning
Properties of jet-medium interaction	q_L	Magnitude of momentum kick along the jet direction per jet-(medium parton) collision
	$f_R\langle N_k\rangle$	Centrality-dependent number of kicked partons per trigger multiplied by the survival factor f_R
	f_J	Ratio of (jet component yield per trigger in A+A collisions) to (associated jet component in pp collisions)
Properties of medium parton momentum distribution in central $A+A$ collisions	a	Falloff parameter of medium parton rapidity distribution in the form $(1-x)^a$
	T	"Temperature" of the medium parton p_t distribution
	m_d	Mass parameter to modify the p_t distribution for low p_t

components,

$$\left[\frac{1}{N_{\rm trig}}\frac{dN_{\rm ch}}{p_t dp_t d\Delta\eta d\Delta\phi}\right]^{AA}_{\rm total} = \left[f_R\frac{2}{3}\langle N_k\rangle\frac{dF}{p_t dp_t\, d\Delta\eta d\Delta\phi}\right]^{AA}_{\rm ridge} + \left[f_J\frac{dN^{pp}_{\rm jet}}{p_t dp_t d\Delta\eta d\Delta\phi}\right]^{AA}_{\rm jet}. \quad (9)$$

To obtain the associated ridge yield in the first term on the right hand side of Eq. (9) for $A+A$ collisions, we need information on the medium parton distribution. We describe the normalized initial medium parton momentum distribution, which implicitly includes all possible physical effects, as represented by [25]

$$\frac{dF}{p_{ti}dp_{ti}dy_i d\phi_i} = A_{\rm ridge}(1-x)^a\frac{e^{-\sqrt{m^2+p_{ti}^2}/T}}{\sqrt{m_d^2+p_{ti}^2}}, \quad (10)$$

where $A_{\rm ridge}$ is a normalization constant defined (and determined numerically) by

$$\int dy_i d\phi_i\, p_{ti}dp_{ti}\,A_{\rm ridge}(1-x)^a\frac{\exp\left\{-\sqrt{m^2+p_{ti}^2}/T\right\}}{\sqrt{m_d^2+p_{ti}^2}} = 1, \quad (11)$$

x is the light-cone variable

$$x = \frac{\sqrt{m^2+p_{ti}^2}}{m_b}e^{|y_i|-y_b}, \quad (12)$$

a is the falloff parameter that specifies the rate of decrease of the distribution as x approaches unity, y_b is the beam parton rapidity, and m_b is the mass of the beam parton. A small value of a indicates a relatively flat rapidity distribution. In particular, a boost-invariant rapidity distribution will be characterized by $a=0$. A large value of $a \gg 1$ indicates a relatively sharp falloff rapidity distribution. As $x \leqslant 1$, there is a kinematic boundary that is a function of y_i and p_{ti} at $x=1$,

$$\sqrt{m^2+p_{ti}^2} = m_b e^{y_b-|y_i|}. \quad (13)$$

We set m_b equal to m_π and y_b equal to y_N, the rapidity of the beam nucleons in the center-of-mass system.

From the above discussions, we note that the momentum-kick model physical parameters can be divided into two categories as given in Table III where the meaning of each parameter is listed. There are parameters q_L, $f_R\langle N_k\rangle$, and f_J that pertain to the jet-medium interaction. They provide information on the momentum kick per collision q_L along the jet direction, the number of jet-(medium parton) collisions $\langle N_k\rangle$ multiplied by f_R, and the ratio f_J of the jet component in $A+A$ collisions per trigger relative to the jet component in pp collisions. Finally, there are parameters a, T, and m_d that pertains to the properties of the medium at the moments of jet-(medium parton) collisions. They provide information on the shape of the early medium parton momentum distribution. The evaluation of these quantities from fundamental theories is beyond the scope of the present theoretical development.

In calculating theoretical differential distribution $dN_{\rm ch}/N_{\rm trig}\,d\Delta\eta$ as a function of $\Delta\eta$, we impose the experimental constraints of $\eta^{\rm trig}_{\rm min} \leqslant \eta^{\rm trig} \leqslant \eta^{\rm trig}_{\rm max}$ and $\eta^{\rm assoc}_{\rm min} \leqslant \eta^{\rm assoc} \leqslant \eta^{\rm assoc}_{\rm max}$ that generate various pseudorapidity differences $\Delta\eta = \eta^{\rm assoc} - \eta^{\rm trig}$. We add up all yields $dN_{\rm ch}/N_{\rm trig}\,d\Delta\eta$ of the same $\Delta\eta = \eta^{\rm assoc} - \eta^{\rm trig}$ to get the uncorrected yield as a function of $\Delta\eta$. We assume that the acceptance is uniform in regions of both $\eta^{\rm assoc}$ and $\eta^{\rm trig}$. Theoretical acceptance-corrected yield is then equal to the product of the uncorrected yield and the acceptance correction factor $f_{\rm acc}(\Delta\eta)$. We can alternatively carry out the acceptance correction as the uncorrected yield divided by the factor $[1/f_{\rm acc}(\Delta\eta)]$ arising from a uniformly generated distribution in $\eta^{\rm trig}$ and $\eta^{\rm assoc}$.

The acceptance correction factor $f_{\rm acc}(\Delta\eta)$ can be obtained from geometrical considerations by plotting the acceptance region in the plane of $\eta^{\rm assoc}$ and $\eta^{\rm trig}$ and changing the axes to $\eta^{\rm assoc}-\eta^{\rm trig}$ and $\eta^{\rm assoc}+\eta^{\rm trig}$. From the geometrical areas after the change of axes, the $\Delta\eta$ acceptance correction factor is given by

$$f_{\rm acc}(\Delta\eta) = \begin{cases} \frac{\left(\eta^{\rm trig}_{\rm max}-\eta^{\rm trig}_{\rm min}\right)}{\Delta\eta-\left(\eta^{\rm assoc}_{\rm min}-\eta^{\rm trig}_{\rm max}\right)} & \text{for } \eta^{\rm assoc}_{\rm min}-\eta^{\rm trig}_{\rm max} < \Delta\eta \leqslant \eta^{\rm assoc}_{\rm min}-\eta^{\rm trig}_{\rm min} \\ 1 & \text{for } \eta^{\rm assoc}_{\rm min}-\eta^{\rm trig}_{\rm min} \leqslant \Delta\eta \leqslant \eta^{\rm assoc}_{\rm max}-\eta^{\rm trig}_{\rm max} \\ \frac{\left(\eta^{\rm trig}_{\rm max}-\eta^{\rm trig}_{\rm min}\right)}{\left(\eta^{\rm assoc}_{\rm max}-\eta^{\rm trig}_{\rm min}\right)-\Delta\eta} & \text{for } \eta^{\rm assoc}_{\rm max}-\eta^{\rm trig}_{\rm max} \leqslant \Delta\eta < \eta^{\rm assoc}_{\rm max}-\eta^{\rm trig}_{\rm min}. \end{cases} \quad (14)$$

TABLE IV. Jet-medium interaction and medium parton distribution parameters in Eqs. (2) and (10) in the momentum-kick model for particles associated with a hadron trigger with different $p_t^{\rm trig}$ in central Au + Au collisions at $\sqrt{s_{NN}} = 200$ GeV.

Centrality		STAR 0–5%	PHOBOS 0–10%	PHENIX 0–20%			
		4–6 GeV	>2.5 GeV				
Hadron trigger	$p_t^{\rm trig}$			2–3 GeV	3–4 GeV	4–5 GeV	5–10 GeV
Momentum kick	q_L		1.0 GeV		0.80 GeV		
Number kicked partons	$f_R\langle N_k\rangle$		3.8		3.0		
Jet component survival factor	f_J		0.632		0.632 for $p_t^{\rm assoc} < 2$ GeV 0.82 for $2 < p_t^{\rm assoc} < 3$ GeV 1.00 for $3\,{\rm GeV} < p_t^{\rm assoc}$		
Medium parton distribution parameters in central Au + Au Collisions	a				0.5		
	T				0.5 GeV		
	m_d				1.0 GeV		

A computer program to carry out the momentum-kick model analysis outlined above can be obtained from the author on request.

V. ANALYSIS OF PHENIX RIDGE DATA

In this section, we investigate the PHENIX near-side ridge data for pp collisions and for the most central (0–20%) Au + Au collisions at $\sqrt{s_{NN}} = 200$ GeV. The region of acceptance includes $|\eta^{\rm trig}, \eta^{\rm assoc}| < 0.35$ and many $p_t^{\rm trig} \otimes p_t^{\rm assoc}$ combinations [14].

We need to find out how the jet component in Au + Au collisions is related to the jet component in pp collisions. Previously, the jet component per trigger in Au + Au collisions can be considered as an attenuated jet component in pp collisions with a survival factor $f_J \sim 0.632$ [25]. For the PHENIX experimental data, we find that f_J increases to unity as $p_t^{\rm assoc}$ increases to 3–4 GeV. We can understand this behavior because the jets with $p_t^{\rm assoc} > 3$–4 GeV are likely to come from the fragmentation process outside the medium and the associated particles are likely to be unattenuated. As $f_J = 0.632$ for $p_t^{\rm assoc} < 2$ GeV and $f_J = 1.0$ for $p_t^{\rm assoc} > 3$ GeV, respectively, we can interpolate $f_J = 0.82$ in the intermediate region and use an empirical f_J factor that depends on $p_t^{\rm assoc}$,

$$f_J\left(p_t^{\rm assoc}\right) = \begin{cases} 0.632 & \text{for} \quad p_t^{\rm assoc} < 2\,{\rm GeV}, \\ 0.82 & \text{for} \quad 2 < p_t^{\rm assoc} < 3\,{\rm GeV}, \\ 1.0 & \text{for} \quad 3\,{\rm GeV} < p_t^{\rm assoc}. \end{cases} \tag{15}$$

With the knowledge of jet component in Au + Au collisions, we can determine the properties of the medium and the characteristics of the jet-medium interaction. For the medium momentum distribution given by Eq. (10), we use the same shape as that obtained previously in the analysis of the STAR ridge data [25] with parameters

$$a = 0.5, \quad T = 0.50\ {\rm GeV}, \quad \text{and} \quad m_d = 1\,{\rm GeV}. \tag{16}$$

The remaining free parameters are then the magnitude of the momentum kick q_L along the jet direction and the number of attenuated medium kicked partons $f_R\langle N_k\rangle$. The PHENIX ridge data are found to be well described (Fig. 1) by

$$q_L = 0.8\ {\rm GeV} \quad \text{and} \quad f_R\langle N_k\rangle = 3.0. \tag{17}$$

We summarize the values of the parameters for the analysis of the PHENIX ridge data in Table IV. As a comparison, we also list the values of the parameters used previously in the analysis of the STAR and PHOBOS ridge data.

In Fig. 1, we show the PHENIX near-side ridge data [14] for collisions at $\sqrt{s_{NN}} = 200$ GeV and the momentum-kick model theoretical results. The solid data point are the total associated particle yield per trigger, $dN_{\rm ch}/N_{\rm trig}\, d\Delta\phi$, in central Au + Au collisions, and the open circles are the associated particle yields per trigger, $dN_{\rm ch}/N_{\rm trig}\, d\Delta\phi$, in pp collisions [14]. Theoretical results are given as various curves. The solid, dashed, and dashed-dot curves are the theoretical total Au + Au associated particle yields per trigger, the Au + Au ridge particle yields per trigger, and the pp associated particle yields, respectively. The different subfigures give the yields of associated particles with different $p_t^{\rm assoc}$, spanning $p_t^{\rm assoc}$ from 0.4 GeV up to $p_t^{\rm trig}$.

Comparison of the PHENIX near-side data with the results of the momentum-kick model in Fig. 1 indicates that the PHENIX ridge data on the near-side for central Au + Au collisions at $\sqrt{s_{NN}} = 200$ GeV [14] can be well described by the momentum-kick model.

We can compare the extracted values of physical parameters of the jet-medium interaction and medium parton characteristics with those extracted previously from the STAR data. The centrality region covered by the present PHENIX measurement [14] extends from 0 to 20%, whereas the STAR data [1] extends from 0 to 5%. The method of subtracting the v_2 background are also different [43]. The STAR detector covers $|\eta| < 1$ and $0 < \phi < 2\pi$; the PHENIX detector covers $|\eta| < 0.35$ and only about half of the full range of azimuthal angles. The medium parton parameters a, T, and m_d are the same, whereas $(q_L,\ f_R\langle N_k\rangle)$ is (1 GeV, 3.8) for the STAR data and (0.8 GeV, 3.0) for the PHENIX data. The difference in q_L and $f_R\langle N_k\rangle$ may arise from difference in centrality selections and the methods of processing the data.

From the present study of the PHENIX ridge data in the region of $|\eta| < 0.35$, we can briefly compare the associated particle yield per trigger of the ridge component and the jet

component in central Au + Au collisions as a function of $p_t^{\rm assoc}$. We find from Fig. 1 that the ridge associated particle yield per trigger is comparable to the jet associated particle yield for $p_t^{\rm assoc} \lesssim 2$ GeV. Thus, ridge particles show up as an excess to the jet component in the region of small $\Delta\eta$ and $\Delta\phi \sim 0$ for $p_t^{\rm assoc} \lesssim 2$ GeV. However, for $p_t^{\rm assoc} > 2$–3 GeV, the jet component dominates over the ridge component. This variation of the relative strengths of the jet and ridge components is reproduced well by the momentum-kick model. The physical reason for the large contribution of the ridge component around $p_t \sim 1$ GeV arises from fact that the ridge momentum distribution is in fact the initial transverse momentum distribution shifted by a momentum of about 1 GeV.

The range of $\Delta\eta$ examined by the PHENIX Collaboration is relatively small. A much larger range of $\Delta\eta$ has been investigated by the STAR and PHOBOS Collaborations. As a function of $\Delta\eta$, the jet component decreases rapidly away from the peak at $(\Delta\phi, \Delta\eta) \sim 0$, whereas the ridge component extends to regions of large $|\Delta\eta|$ and it dominates over the jet component at $|\Delta\eta|$, as observed by the STAR [5] and PHOBOS Collaborations [17]. This feature in the variation in $\Delta\eta$ is also reproduced by the momentum-kick model [25].

As the jet component in Au + Au collisions per trigger is related to the associated particles in pp collisions, and the characteristics of the associated particles in pp collision change significantly as $p_t^{\rm trig}$ changes, so the jet component per trigger in the Au + Au collision also changes its properties significantly as $p_t^{\rm trig}$ changes. The temperature $T_{\rm jet}$ and the number of these associated particles $N_{\rm jet}$ increases linearly with $p_t^{\rm trig}$.

In contrast to the large variation of the properties of the jet component as a function of $p_t^{\rm trig}$, physical parameters associated with the medium partons appears to be relatively robust, independent of $p_t^{\rm trig}$. The same set of medium property parameters of a, T, and m_d apply to the medium parton momentum distribution for all $p_t^{\rm trig}$ and $p_t^{\rm assoc}$ combinations. They coincide also with those from STAR and PHOBOS measurements [25]. The robust nature of these physical quantities enhances their quality as basic properties of the produced medium. The falloff parameter $a = 0.5$ for the distribution $(1-x)^a$ of Eq. (10) reveals that the early medium parton rapidity distribution is relatively flat but not boost-invariant, which would correspond to $a = 0$. The $(1-x)^a$ distribution with the kinematic limit of $x = 1$ indicates that the distribution is in the shape of a rapidity plateau, as shown in Fig. 6(b) of Ref. [25]. The temperature parameter $T = 0.5$ GeV shows that it is a thermal-like distribution with a temperature between those of a high-p_t jet and the bulk matter. The quantity $m_d = 1$ GeV indicates a small modification of the thermal distribution at lower p_t.

Similarly, the set of physical parameters that describe the jet-medium interaction, q_L and $f_R\langle N_K\rangle$, appear also to be robust as the same set can describe the ridge component for all different $p_t^{\rm trig}$ and $p_t^{\rm assoc}$ combinations. The extracted magnitude of the momentum kick is $q_L = 0.8$ GeV per jet-(medium parton) collision, and the number of jet-medium parton collision for the most central collisions multiplied by the survival factor is 3.

There is, however, a difference of about 20% in the values of q_L and $f_R\langle N_K\rangle$ extracted from the PHENIX near-side ridge data, compared to those extracted from the STAR near-side ridge data. This difference may reflect the difference in centrality selection and the degree of uncertainty in processing the experimental data.

VI. THE NATURE OF THE SCATTERING BETWEEN THE JET PARTON AND THE MEDIUM PARTON

We have extracted the relevant physical quantities from the ridge data. We come to the second stage of our analysis to find out the nature of the collision between the jet parton and the medium parton. We also wish to correlate the extracted physical quantities to those in relevant physical phenomena to see whether they are consistent. We shall discuss the extracted magnitude of the momentum kick q_L in this section, the extracted shape of the rapidity distribution in Sec. VII, and the extracted number of kicked partons in Sec. VIII.

The extracted magnitude of the momentum kick q_L is the longitudinal momentum imparted by the jet parton onto the medium parton per collision, along the jet direction. This quantity q_L is also the longitudinal momentum loss of the incident jet parton in the parton-parton collision. We find $q_L = 0.8$ GeV for the present set of PHENIX data with 20% centralitiy and $q_L = 1.0$ GeV previously for the STAR ridge data with 0–5% centrality. The average q_L value from the two measurements is $q_L = 0.9$ GeV.

To study the scattering between the jet parton and the medium parton, we relate the longitudinal momentum loss q_L of the jet to its momentum transfer squared t. The latter quantity is related to the scattering correlation length a in an elastic parton-parton collision, for which many pieces of information have been obtained previously [46,47,50–60].

It is convenient to work in the medium rest frame in which the average velocity of the medium partons is zero. We consider the collision of an energetic jet parton a with an medium parton b at rest, which represents an average parton of the medium. For simplicity, we specialize to the case in which all partons have the same rest mass m. The elastic scattering of the jet parton a with the medium parton b leads to partons c and d as

$$a + b \to c + d. \tag{18}$$

The square of the center-of-mass energy of the colliding partons is

$$s = (a+b)^2 = 2m^2 + 2m\sqrt{\mathbf{a}^2 + m^2}, \tag{19}$$

where we have used the same label for a parton and its three- and four-momentum. In the elastic scattering, the momentum transfer squared $t = (a-c)^2$ is

$$t = -\tfrac{1}{2}(s - 4m^2)(1 - \cos\theta^*) \tag{20}$$

where θ^* is the scattering angle between $\mathbf{c}^*$ and $\mathbf{a}^*$ and the superscript $*$ denotes quantities in the $(a+b)$ center-of-mass system. There is thus a relation between the scattering angle θ^* and the momentum transfer t. The maximum and minimum

values of t are

$$t_{\max} = 0, \quad \text{for } \theta^* = 0,$$
$$t_{\min} = -(s - 4m^2), \quad \text{for } \theta^* = \pi. \tag{21}$$

After the elastic parton-parton scattering, parton a becomes parton c with the same energy and the magnitude of the three-momentum,

$$|\mathbf{c}^*| = \tfrac{1}{2}\sqrt{s - 4m^2}. \tag{22}$$

The longitudinal component of c in the center-of-mass system is

$$c_z^*(\theta^*) = \tfrac{1}{2}\sqrt{s - 4m^2}\cos\theta^*. \tag{23}$$

Transforming back to the medium rest frame, one obtains the longitudinal momentum c_z of the final parton in the medium rest frame to be

$$c_z(\theta^*) = \gamma[c_z^*(\theta^*) + \beta c_0^*], \tag{24}$$

where the Lorentz transformation factors γ and β are $\gamma = \sqrt{s}/2m$ and $\beta = \sqrt{1 - \gamma^{-2}}$. The final momentum of c_z for the case of $\theta^* = 0$ gives the initial longitudinal momentum of the incident parton $a_z = c_z(\theta^* = 0)$. Therefore, the momentum loss of the incident jet parton in the medium rest frame is

$$q_L = c_z(\theta^* = 0) - c_z(\theta^*) = -\frac{t}{2m}\frac{\sqrt{s}}{\sqrt{s - 4m^2}}. \tag{25}$$

In the elastic parton-parton scattering, the longitudinal momentum loss q_L of the incident jet parton is equal to the longitudinal momentum gain or momentum kick q_L suffered by the medium parton along the jet direction. Thus, for a given incident parton with a definite parton-parton center-of-mass $\sqrt{s}$, the knowledge of the magnitude of the momentum kick q_L will provide information on the momentum transfer squared $|t|$.

In detecting a trigger of energy 4–6 GeV, the incident jet parton has an energy of order 10 GeV, as the partons loses about a few GeV in kicking a few medium partons. For this incident parton momentum of order $p_t^{\text{jet}} \sim 10$ GeV in our present experimental setup, $\sqrt{s} \gg m$ and $q_L \sim |t|/2m$, which is independent of the parton energy. For $q_L = 0.9$ GeV extracted from the momentum-kick model, we therefore obtain the squared momentum transfer t to have the magnitude

$$|t| = 2mq_L\frac{\sqrt{s - 4m^2}}{\sqrt{s}} = 0.255 \text{ GeV}^2. \tag{26}$$

As the longitudinal momentum gained by the medium parton in the momentum-kick model is an average quantity, the corresponding t in Eq. (26) should be considered as an average value $\langle|t|\rangle$.

The extracted value of the (average) momentum transfer squared $|t|$ in the parton-parton collision is small, substantially less than 1 GeV^2. This suggests that the collision process is nonperturbative. The parton-parton scattering should be more appropriately described by the exchange of a nonperturbative pomeron [50–60].

We would like to relate the (average) momentum transfer squared t to a correlation length a by considering a parton-parton collision profile function of the form

$$\Gamma(\mathbf{b}) = \frac{\Gamma_0}{2\pi a^2}\exp\left\{-\frac{\mathbf{b}^2}{2a^2}\right\}, \tag{27}$$

where Γ_0 is the scattering strength parameter. The scattering amplitude is

$$f(\mathbf{q}_t) = \frac{ik}{2\pi}\int d\mathbf{b}e^{i\mathbf{q}_t\cdot\mathbf{b}}\Gamma(\mathbf{b}) = \frac{ik}{2\pi}\frac{\Gamma_0 a^2}{2\pi}\exp\left\{-\frac{a^2\mathbf{q}_t^2}{2}\right\}. \tag{28}$$

As $\mathbf{q}_t^2 = -t - t^2/(s - 4m^2) \sim -t$, the elastic parton-parton scattering differential cross section is

$$\frac{d\sigma}{dt} \sim \frac{\Gamma_0 a^4}{8\pi^2}e^{a^2 t}. \tag{29}$$

The average value of $|t|$ is therefore

$$\langle|t|\rangle = \int_{t_{\min}}^{t_{\max}}|t|\frac{d\sigma}{dt}\Big/\int_{t_{\min}}^{t_{\max}}\frac{d\sigma}{dt} \sim \frac{1}{a^2}, \tag{30}$$

which allows us to infer the magnitude of the correlation length a from the average value of momentum transfer squared $\langle|t|\rangle$. From Eqs. (30) and (26), the magnitude of the longitudinal momentum kick q_L extracted from the ridge data corresponds to a parton-parton scattering correlation length a of

$$a \sim 1/\sqrt{\langle|t|\rangle} = 0.39 \text{ fm}. \tag{31}$$

Is this correlation length a compatible with measurements of the same quantity in other descriptions of the parton-parton elastic collision process? One can consider a model of hadron-hadron collisions in which the partons of one hadron collide with partons of the other hadron, as in the Chou-Yang model [47]. In the original Chou-Yang droplet model [47], the partons are assumed to be pointlike without any structure of a correlation length. The Chou-Yang model of the pointlike parton-parton scattering can be generalized to the case of partons with a finite correlation length, with the parton-parton scattering differential cross section assuming the form of Eq. (29) [46,48,49]. The elastic hadron-hadron elastic differential cross section in the modified Chou-Yang model then takes the form [46]

$$\frac{d\sigma_{\text{hadron-hadron}}}{dt} = AF_p^2(t)F_t^2(t)|A_{qq}(t)|^2, \tag{32}$$

where A is a normalization factor; $F_p(t)$ and $F_t(t)$ are the projectile and target hadron form factors, respectively; and $|A_{qq}(t)|^2$ is the quark-quark scattering matrix element taken to have the same functional form as Eq. (29), [46,48,49]

$$|A_{qq}(t)|^2 = e^{a^2 t}. \tag{33}$$

Experimental pp, $\pi^+ p$, and $\pi^- p$ elastic differential cross sections at 200 GeV can be well described by

$$a = \begin{cases} 0.33 \text{ fm} & \text{for } pp \text{ collisions;} \\ 0.25 \text{ fm} & \text{for } \pi p \text{ collisions.} \end{cases} \tag{34}$$

(see Fig. 14 and Table X of Ref. [46], where the correlation length a is represented in terms of the "quark radius r_q" with $r_q = \sqrt{2}a$.)

It is of interest to inquire further whether the correlation length (31) extracted from the ridge data is compatible with the correlation length in the nonperturbative description of the pomeron, for which much progress has been made in recent years. The slow rise of the total hadron-hadron cross sections with increasing energy as $(\sqrt{s})^{0.0808}$ in high-energy hadron-hadron collisions suggests that the scattering process is dominated by the exchange of a pomeron whose quantum numbers are those of the vacuum [59,60,64]. The approximate validity of the additive quark model, where the cross section is proportional to the valence quark number, suggests that the exchange of the pomeron takes place as the exchange between single quark partons.

In QCD, it is natural to assume that the exchange of the pomeron between constituent quark partons is just the exchange of a cluster of two or more gluons to get the correct quantum number of the vacuum [92–94]. In perturbative QCD, the perturbative exchange of two gluons between quark partons leads to a singularity of the elastic hadron-hadron scattering amplitude at $t = 0$, and it does not reproduce the experimental t dependence. The experimental differential cross section, $d\sigma_{\text{hadron}-\text{hadron}}/dt$ corresponds more properly to the hadron form factors, as in Eq. (32), with the cluster of exchanged gluons coupled to a single quark. It is more appropriate to describe the exchange of the pomeron to be a nonperturbative process and take into account nonperturbative properties of the QCD vacuum.

The nonperturbative QCD vacuum can be described as consisting of a gluon condensate of a color field strength characterized by [95]

$$\left\langle g^2 F^C_{\mu\nu}(0) F^{C,\mu\nu}(0)\right\rangle_A = M_c^4, \tag{35}$$

where the expectation value is taken with respect to the nonperturbative vacuum and $M_c = (0.9 \pm 0.1\ \text{GeV})$ [96]. For the description of the pomeron in the scattering process, Landshoff and Nachtmann [50,51] generalized the concept of the gluon condensate to the case of a gluon condensate with a finite correlation length a associated with each colliding parton,

$$\left\langle g^2 F^C_{\mu\nu}(x) F^{C,\mu\nu}(y)\right\rangle_A = M_c^4 f((x-y)^2/a^2), \tag{36}$$

where $x - y$ is spacelike with $(x-y)^2 < 0$. From hadron spectroscopy and the total cross section at high energies, the correlation length was estimated to be [51,53]

$$a \approx 0.4\,\text{fm}. \tag{37}$$

A parton-parton scattering is then described as taking place by the scattering of the parton on the condensate that is associated with the collided partons, as in potential scattering.

The concept of correlators with a correlation length was further developed in QCD in the model of stochastic vacuum (MSV) [52]. In this model, the gluon condensate correlator is assumed to be described by invariant functions D and D_1 that are normalized to $D(0) = D_1(0) = 1$. They are given explicitly in Refs. [54,56] and they fall off rapidly on a scale of the correlation length a. The correlators are separated into a part of strength κ that is non-Abelian and a part of strength $(1-\kappa)$ that is Abelian [54,55],

$$\begin{aligned}
&\left\langle g^2 F^C_{\mu\nu}(x) F^D_{\rho\sigma}(y)\right\rangle \\
&= \delta^{CD}\frac{\pi^2 G_2}{6}\left\{\kappa(\delta_{\mu\rho}\delta_{\nu\sigma} - \delta_{\mu\sigma}\delta_{\nu\rho}) D\left[\frac{(x-y)^2}{a^2}\right]\right. \\
&\quad + (1-\kappa)\frac{1}{2}\left[\frac{\partial}{\partial z_\mu}(z_\rho\delta_{\nu\sigma} - z_\sigma\delta_{\nu\rho}) + \frac{\partial}{\partial z_\nu}(z_\sigma\delta_{\nu\rho} - z_\rho\delta_{\nu\sigma})\right] \\
&\quad \left.\times D_1\left[\frac{(x-y)^2}{a^2}\right]\right\},
\end{aligned} \tag{38}$$

where C and D are color indices and $\pi^2 G_2/6 = M_c^4$. Differential hadron-hadron cross sections for high-energy elastic scattering have been analyzed and the experimental data can be described well by using a condensate correlator with parameters [56]

$$\begin{aligned}
a &= 0.32\ \text{fm}, \\
\kappa &= 0.74, \\
\text{and}\ \ G_2 &= (0.529\ \text{GeV})^4.
\end{aligned} \tag{39}$$

The properties of the gluon condensate can be further examined by lattice gauge calculations. The correlation length parameter a, the non-Abelian parameter κ, and the gluon condensate strength G_2 in Eq. (39) obtained in quenched lattice calculations [57,58] are compatible with those obtained in hadron-hadron differential cross sections [56].

We can summarize the values of the correlation length a in a parton-parton collision from different investigations in Table V.

TABLE V. Comparison of the correlation length a obtained from various considerations.

Source	Correlation length a (fm)	References
Momentum-kick model	0.39	Present investigation
Small $\lvert t\rvert$ hadron-hadron $d\sigma/dt$	0.33 (pp)	[46]
in modified Chou-Yang Model	0.25 (πp)	[46]
Hadron spectroscopy & σ_{tot}	$\approx$0.40	[51,53]
in stochastic vacuum model		
Small $\lvert t\rvert$ hadron-hadron $d\sigma/dt$	0.32	[56]
in stochastic vacuum model		
Gluon correlators	0.22–0.48	[58]
in lattice gauge calculations		

It is gratifying that the correlation length estimated from the ridge data, $a = 0.39$ in Eq. (31), is compatible with the value of $a = 0.25$–0.33 fm in Eq. (34), obtained in a hadron-hadron elastic scattering in the modified Chou-Yang model [46]; the value of $a \approx 0.4$ fm in Eq. (37), obtained from hadron spectroscopy and total cross sections in the model of stochastic vacuum [53]; the value of $a = 0.32$ fm in Eq. (39), obtained in the nonperturbative pomeron description in the model of stochastic vacuum [56]; and the value of $a = 0.22$–0.48 fm obtained in lattice gauge calculations [58]. The approximate agreement of the correlation length extracted in the momentum-kick model (31) with many previous results

supports the approximate validity of the magnitude of the momentum kick q_L in the present analysis.

Because of the small value of $|t| < 1$ GeV and the compatibility of of the correlation length a with previous description of the nonperturbative pomeron, we conclude that the parton-parton scattering between the jet parton and the medium parton arises from the exchange of a nonperturbative pomeron, in the momentum range of $p_t^{\rm trig} < 10$ GeV considered in the near-side ridge measurements. Our ability to ascertain the nature of the parton-parton scattering will help us select the proper description to formulate the process of energy loss for these jet partons.

VII. THE OCCURRENCE OF THE RAPIDITY PLATEAU

The initial momentum distribution of the medium partons in Eq. (10), $(1-x)^a \exp\{-\sqrt{m^2+p_t^2}/T\}/\sqrt{m_d^2+p_t^2}$, gives an early parton momentum distribution that has three prominent features. First, it has a thermal-like transverse distribution whose characteristic slope parameter T is between those of the jet and the bulk inclusive matter. Second, the rapidity distribution is relatively flat around $y \sim 0$. Third, the rapidity distribution is quite extended, reaching out to large rapidities.

Questions may be raised with regard to the occurrence of the rapidity plateau in the early parton momentum distribution. One immediate question is whether such a plateau structure also occurs in the distribution of produced particles in related phenomena. Theoretically, the rapidity plateau occurs in elementary processes involving the fragmentation of flux tubes [62–64] and in many particle production models such as models based on preconfinement [65], parton-hadron duality [66] cluster fragmentation [67], string-fragmentation [68], dual-partons [69], the Venus model [70], the RQMD model [71], multiple collision model [72], parton cascade model [73,74], color-glass condensate model [75], the AMPT model [76], the Lexus model [77], and many other models. To investigate the origin of the rapidity plateau in a quantum mechanical framework, we can go a step further to use the physical argument of transverse confinement to establish a connection between QCD and QED2 [25,26]. One finds that a rapidity plateau of produced particles is a natural occurrence when color charges pull away from each other at high energies [61–64] as in QED2 [78–81]. Experimental evidence for a plateau in rapidity distributions along the sphericity axis or the thrust axis has been observed earlier in $\pi^{\pm}$ production in high-energy $e^{\pm}$ annihilation [82–86] and in pp collisions at Relativistic Heavy Ion Collider (RHIC) energies [87].

To gain a new insight into the rapidity plateau structure of the early partons, it is of interest to compare the shape of the rapidity distribution of the early partons extracted in the momentum-kick model with those from pp and central Au + Au collisions at the same energy, $\sqrt{s_{NN}} = 200$ GeV. We plot in Fig. 2 these rapidity distributions normalized to the rapidity at $y = 0$, after integrating over the p_t distributions. The data points are from the BRAHMS Collaboration [87] and the solid curve is dN/dy extracted from the momentum-kick model as given by Eq. (10). One observes that the rapidity distributions for pp collisions have the greatest plateau width

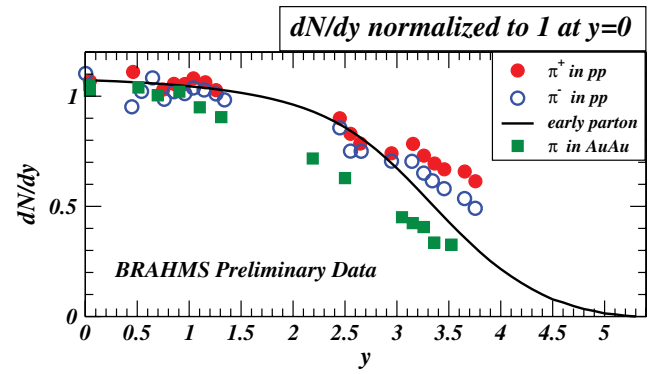

FIG. 2. (Color online) The data points are the pion rapidity distributions for pp and Au + Au collisions from the BRAHMS Collaboration. The solid curve is the early parton momentum rapidity distribution extracted from the ridge data associated with the near-side jet.

in y, while the early parton rapidity distribution has a slightly narrower plateau width and is in between those of the pp and Au + Au central collisions. This is consistent with the evolution of the partons from a pp-like distribution to the early parton distribution and eventually to the inclusive nucleus-nucleus rapidity distribution that is closer to a Gaussian shape than a plateau shape. The comparison indicates that the rapidity distribution extracted here during the early moments of jet-medium interactions is at an intermediate stage in the dynamical evolution process. Such a viewpoint is further supported by the observation that the p_t slope parameter of the early partons (the ridge particles) is in between those of the jet and the inclusive central Au + Au distributions [3].

VIII. THE CENTRALITY DEPENDENCE OF THE RIDGE YIELD

The momentum-kick model also provides information on the number of attenuated kicked partons, $f_R\langle N_k\rangle$, for the most central collisions. It is of interest to examine whether these number of kick partons in the most central collision is consistent with the centrality dependence of the ridge yield. One can follow the trajectory of the jet, using the extracted number of kicked partons as a normalization for the most central collision and infer the ridge yield as a function of the centrality, to investigate whether the momentum-kick model can also describe the ridge yield at other centralities.

As the centrality dependence of the ridge yield has not been investigated in connection with the PHENIX ridge data of Ref. [14], we shall use the STAR centrality data [3] to discuss the centrality dependence. We review here the description of the centrality dependence in the momentum-kick model. We wish to show here that the extracted number of partons kicked by the jet is also consistent with other related phenomenon.

The momentum-kick model separates the ridge yield into a geometrical factor part that depends on the average number of kicked partons $2f_R\langle N_k\rangle/3$ and another factor of differential distribution $EdF/d\mathbf{p}$ in Eq. (2). The quantity $\langle N_k\rangle$ depends on the centrality.

We consider a jet source point at $\mathbf{b}_0$, from which a midrapidity jet parton originates. The number of jet-(medium parton) collisions along the jet trajectory, which makes an angle ϕ_s with respect to the reaction plane, is [25]

$$N_k(\mathbf{b}_0, \phi_s) = \int_0^\infty \sigma\, dl \frac{dN_{\rm parton}}{dV}[\mathbf{b}'(\mathbf{b}_0, \phi_s)], \tag{40}$$

where $0 < l < \infty$ parametrizes the jet trajectory, σ is the jet-(medium parton) scattering cross section, and $dN_{\rm parton}(\mathbf{b}')/dV$ is the parton density of the medium at $\mathbf{b}'$ along the trajectory l.

Jet-(medium parton) collisions take place along different parts of the trajectory at different l and involve the medium at different stages of the expansion. They depend on the space-time dynamics of the jet and the medium. Assuming hydrodynamical expansion of the fluid in both the longitudinal and transverse directions and focusing our attention on midrapidity, we can determined the distribution of the number of jet-(medium parton) collisions $P(N)$ as a function of the transverse jet source point coordinate $\mathbf{b}_0$ and the azimuthal angle ϕ_s [25]. We need to weight the number of kicked medium particles by the local binary collision number element $d\mathbf{b}_0 \times dN_{\rm bin}/d\mathbf{b}_0$. The normalized probability distribution $P(N, \phi_s)$ with respect to the number of ridge particles [or jet-(medium parton) collisions] is

$$P(N, \phi_s) = \frac{1}{N_{\rm bin}} \int d\mathbf{b}_0 \frac{dN_{\rm bin}}{d\mathbf{b}_0}(\mathbf{b}_0)\delta[N - N_k(\mathbf{b}_0, \phi_s)]. \tag{41}$$

Thus, the number of ridge particle yield per trigger particle [or the number of jet-(medium parton) collisions per trigger] at an azimuthal angle ϕ_s, averaged over all source points of binary collisions at all $\mathbf{b}_0$ points, is [25]

$$\bar{N}_k(\phi_s) = \int N P(N, \phi_s) e^{-\zeta N} dN \Big/ \int P(N, \phi_s) e^{-\zeta N} dN, \tag{42}$$

where ζ is the exponential index in the ratio of the fragmentation function after N jet-(medium parton) collisions relative to the fragmentation function before any collision,

$$e^{-\zeta N} = \frac{D(p^{\rm trig}, \mathbf{p}_j - \sum_n^N \mathbf{q}_n - \Delta_r)}{D(p^{\rm trig}, \mathbf{p}_j)}. \tag{43}$$

where $\mathbf{q}_n$ is the momentum loss at the nth jet-(medium parton) collision and Δ_r is the momentum loss owing to gluon radiation. From these equations, we get the ridge yield $\bar{N}_k(\phi_s)$ per trigger as

$$\bar{N}_k(\phi_s) = \frac{1}{N_{\rm bin}} \int d\mathbf{b}_0 N_k(\mathbf{b}_0, \phi_s) e^{-\zeta N_k} \times \frac{dN_{\rm bin}}{d\mathbf{b}_0} \Big/ \frac{1}{N_{\rm bin}} \int d\mathbf{b}_0 e^{-\zeta N_k} \frac{dN_{\rm bin}}{d\mathbf{b}_0}. \tag{44}$$

We get the jet quenching measure [25]

$$R_{AA}(\phi_s) = \frac{N_{\rm trig}}{N_{\rm bin}} = \int P(N, \phi_s) e^{-\zeta N} dN = \sum_{N=0}^{N_{\rm max}} P(N, \phi_s) e^{-\zeta N}, \tag{45}$$

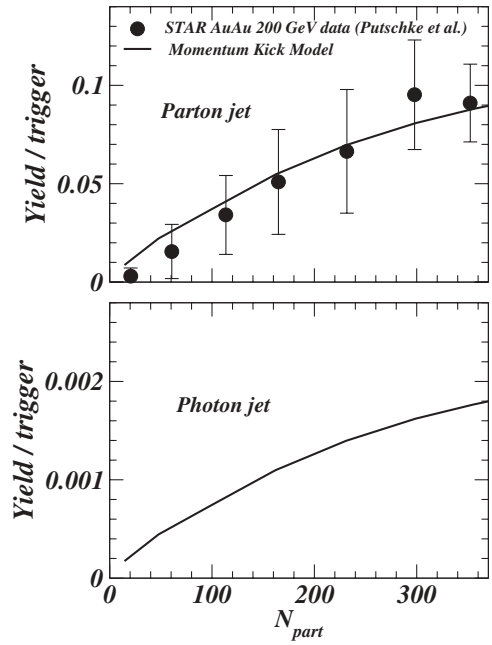

FIG. 3. The total yield of charged ridge particles per parton (hadron) jet (a), and per photon jet (b), as a function of the number of participants. In Fig. 3(a), the data points are from Ref. [3].

which can also be obtained as

$$R_{AA}(\phi_s) = \frac{1}{N_{\rm bin}} \int d\mathbf{b}_0 \exp\{-\zeta N_k(\mathbf{b}_0, \phi_s)\} \frac{dN_{\rm bin}}{d\mathbf{b}_0}. \tag{46}$$

After $\bar{N}_k(\phi_s)$ and $R_{AA}(\phi_s)$ have been evaluated, we can average over all azimuthal angles ϕ_s and obtain the ridge particles [or jet-(medium parton) collisions] per trigger

$$\langle N_k \rangle = \int_0^{\pi/2} d\phi_s \bar{N}_k(\phi_s)/(\pi/2), \tag{47}$$

and

$$\langle R_{AA} \rangle = \int_0^{\pi/2} d\phi_s R_{AA}(\phi_s)/(\pi/2), \tag{48}$$

which is usually expressed just as R_{AA}.

In our previous analysis of the STAR ridge yield and jet quenching, we find that assuming $f_R = f_J = 0.632$, the experimental data of the centrality dependence of R_{AA} and the centrality dependence of the ridge yield using hadron trigger can be explained well when we use [25]

$$\zeta = 0.20 \quad \text{and} \quad \sigma = 1.4\,\text{mb}. \tag{49}$$

The STAR data of ridge yield per trigger as a function of the number of participants are shown in Fig. 3(a) and are compared with the momentum-kick model results [25], for the acceptance of the STAR Collaboration in Ref. [3]. Figure 3(a) shows that the number of kicked partons extracted from the most central collision lead us to a consistent description of the centrality dependence of the ridge yield, an attenuation index ξ that is consistent with the fragmentation and energy loss [25], and a cross section of 1.4 mb. Note that such a cross section is slightly smaller but is of the same order of magnitude, as πa^2

of the correlation length extracted from the momentum-kick model in Eq. (31). As the total elastic-scattering cross section is a product of the geometrical cross section and the strength of the potential inside the correlated region [Eq. (116) of Ref. [97]], the difference of the cross section in Eq. (49) and πa^2 may provide information on the depth of the nonperturbative potential relative to which the parton scatters.

IX. RIDGE PARTICLE YIELD FROM A PHOTON JET

One can consider experiments with two transverse jets in which one of the two jets is a photon jet on the near side while the other jet is a strongly interacting parton on the away side. The use of a near-side photon jet allows one to probe the origin of the ridge particles as we discussed in Sec. I [89]. If the ridge arises from the medium as a result of the collision of the near-side jet, as in the momentum-kick model, the substitution of a photon jet for a hadron jet will lead to a greatly reduced yield of the ridge particles. However, if the ridge particles arise from "several extra particles deposited by forward-backward beam jets into the fireball" [27] or from the backsplash model [33], then the ridge particles yield will not be significantly reduced.

We can make a quantitative estimate of the ridge yield in the momentum-kick model for a photon jet that arises from hard scattering. The number of ridge particles depends on the jet-(medium parton) cross section and the attenuation index ζ. For the high-p_t photon jet, the photon jet-(medium parton) cross section is

$$\sigma(\text{photon} - \text{parton}) = \left(\frac{\alpha_e}{\alpha_s}\right)^2 \sigma(\text{parton} - \text{parton}), \tag{50}$$

where $\alpha_e = 1/137$ is the fine-structure constant. We can take $\alpha_s = 0.2$ as the strong-interaction coupling constant. With $\sigma(\text{parton} - \text{parton}) \sim 1.4$ mb as given by Eq. (49), we can estimate

$$\sigma(\text{photon} - \text{parton}) = 1.86\ \mu b. \tag{51}$$

As the average number of collisions is much less than 1, we can take $\zeta = 0$ in Eq. (44) without much error. One finds that the ridge yield per photon trigger is then

$$\langle N_k \rangle = \frac{1}{N_{\text{bin}}} \int \frac{d\phi_s}{(\pi/2)} d\mathbf{b}_0 N_k(\mathbf{b}_0, \phi_s) \frac{dN_{\text{bin}}}{d\mathbf{b}_0}. \tag{52}$$

We can evaluate $N_k(\mathbf{b}_0, \phi_s)$ by using Eq. (40) and the photon-(medium parton) cross section of Eq. (51) and obtain the total number of ridge particle yield per photon jet as a function of the participant number shown in Fig. 3(b), for the acceptance region as in Ref. [3]. The yield for the photon jet is about 0.002 per photon jet for the most central Au + Au collision, which is small indeed. For all practical purposes, a high-p_t photon jet does not lead to significant production of ridge particles in the momentum-kick model.

X. CONCLUSION AND DISCUSSIONS

Using the momentum-kick model, we examine the PHENIX near-side ridge particle data for central Au + Au collisions at $\sqrt{s_{NN}} = 200$ GeV that cover the range of pseudorapidity, $|\eta| < 0.35$, and a large number of $p_t^{\text{trig}} \otimes p_t^{\text{assoc}}$ combinations. We find that the PHENIX data can be described by the momentum-kick model.

With the successful analysis of the ridge data from STAR, PHOBOS, and PHENIX Collaborations, it is of great interest to find out whether the extracted physical quantities are compatible with those in other relevant physical phenomena. The most important quantity extracted is the (average) magnitude of the longitudinal momentum kick q_L along the jet direction imparted on the medium parton by the jet parton in a parton-parton collision. We find that such a quantity is related to the momentum transfer squared t of the incident jet parton. The magnitude of $|t|$ is less than 1 GeV^2, indicating that the scattering is within the realm of nonperturbative QCD. The scattering of the jet parton and a medium parton is characterized by a correlation length of $a = 0.39$ fm.

On the theoretical side, the correlation length a in parton-parton scattering has been previously obtained in many previous analyses of hadron-hadron elastic differential cross sections and the model the nonperturbative pomeron. The modified Chou-Yang model [46], the model of the nonperturbative pomeron in terms of the stochastic vacuum [56], and lattice gauge calculations of the gluon condensate correlator in Refs. [56,58] give a correlation lengths in the range 0.25–0.37 fm, compatible with the magnitude of the correlation length extracted in the momentum-kick model. It is reasonable to conclude that the parton-parton scattering between the jet parton and the medium parton arises from the exchange of a nonperturbative pomeron.

It should be emphasized that our ability to ascertain the nonperturbative nature of the parton-parton scattering is important in helping us select the proper description for the dynamics of the interaction of the jet and the medium. For jet partons in the momentum range of $p_t^{\text{jet}} < 10$ GeV as considered in measurements involving associated particles, a plausible description needs to include the nonperturbative aspects of the scattering between the jet parton and the medium parton, if one wishes to describe the jet momentum loss and the scattered medium partons properly.

We can examine further the shape of the rapidity plateau in the early parton momentum distribution obtained here. The presence of a rapidity plateau in early history of a central nucleus-nucleus collision as inferred from the momentum-kick model is not a surprising result, as the rapidity plateau structure occurs in elementary process involving the fragmentation of flux tubes [61–64,68] and in many particle production models [65–77]. Experimental evidence for a plateau in rapidity distributions has been observed earlier in $\pi^{\pm}$ production in high-energy e^+-e^- annihilation [82–86] and in pp collisions at RHIC energies [87]. A comparison of the plateau structure of pp, central Au + Au, and early parton distributions in Fig. 2 places rapidity distribution extracted here as an intermediate stage of the dynamical evolution process, just as indicated by the intermediate value of the inverse slope of the ridge particles between those of the jet and the inclusive particles.

The number of kicked partons extracted here also provide the proper normalization to explore the centrality dependence of the ridge yield, whereas the attenuation index ξ is compatible with the estimates from fragmentation process of the jet parton.

It is of interest to propose the use of high-p_t photon jets to examine the associated particles. In the momentum-kick model, the collision of a high-p_t hadron jet with the medium partons lead to the recoil of the medium partons that subsequently materialize as ridge particles. However, for a high-p_t photon jet the photon-(medium parton) cross section is greatly reduced, leading to a much smaller number of produced ridge particles. Thus, a photon jet on the near-side will lead to a very small yield of ridge particles. Such a feature may be used to discriminate among different models.

In summary, we have analyzed PHENIX near-side ridge data for central Au + Au collisions at $\sqrt{s_{NN}} = 200$ GeV. We found that the data can be described well by the momentum-kick model and the extracted physical quantities provide useful information on the nucleus-nucleus collision process. Specifically, the scattering between the jet parton and the medium parton arises from the exchange of a nonperturbative pomeron for $p_t^{\text{jet}} < 10$ GeV. This, however, is only the first two step in the theoretical analysis. The final third step consists of the construction of theoretical models that can explain these physical quantities. Another step is to connect the observed physical quantities to other observables such as the momentum distribution of the bulk matter at subsequent stages of the nucleus-nucleus collision. The momentum-kick model can be further improved with additional inclusion of other effects such as the collective flow, a better description of the elementary jet-(medium parton) collision processes, and perhaps a better Monte Carlo tracking of the jet trajectory and kicked partons.

ACKNOWLEDGMENTS

The author thanks Drs. Vince Cianciolo, Fuqiang Wang, Jiangyong Jia, and Chin-hao Chen for helpful discussions and communications. This research was supported in part by the Division of Nuclear Physics, US Department of Energy, under Contract No. DE-AC05-00OR22725, managed by UT-Battelle, LLC.

[1] J. Adams *et al.* (STAR Collaboration), Phys. Rev. Lett. **95**, 152301 (2005).
[2] J. Adams *et al.* (STAR Collaboration), Phys. Rev. C **73**, 064907 (2006).
[3] J. Putschke (STAR Collaboration), J. Phys. G **34**, S679 (2007).
[4] J. Bielcikova (STAR Collaboration), J. Phys. G **34**, S929 (2007).
[5] F. Wang (STAR Collaboration), invited talk at the XIth International Workshop on Correlation and Fluctuation in Multiparticle Production, Hangzhou, China, November 2007 [arXiv:0707.0815].
[6] J. Bielcikova (STAR Collaboration), J. Phys. G **34**, S929 (2007); J. Bielcikova (STAR Collaboration), talk presented at 23rd Winter Workshop on Nuclear Dynamics, Big Sky, Montana, USA, 11–18 February 2007, arXiv:0707.3100; J. Bielcikova (STAR Collaboration), talk presented at XLIII Rencontres de Moriond, QCD and High Energy Interactions, La Thuile, 8–15 March 2008, arXiv:0806.2261.
[7] B. Abelev (STAR Collaboration), talk presented at 23rd Winter Workshop on Nuclear Dynamics, Big Sky, Montana, USA, 11–18 February 2007, arXiv:0705.3371.
[8] L. Molnar (STAR Collaboration), J. Phys. G **34**, S593 (2007).
[9] R. S. Longacre (STAR Collaboration), Int. J. Mod. Phys. E **16**, 2149 (2007).
[10] C. Nattrass (STAR Collaboration), J. Phys. G **35**, 104110 (2008).
[11] A. Feng (STAR Collaboration), J. Phys. G **35**, 104082 (2008).
[12] P. K. Netrakanti (STAR Collaboration), J. Phys. G **35**, 104010 (2008).
[13] O. Barannikova (STAR Collaboration), J. Phys. G **35**, 104086 (2008).
[14] A. Adare *et al.* (PHENIX Collaboration), Phys. Rev. C **78**, 014901 (2008).
[15] M. P. McCumber (PHENIX Collaboration), J. Phys. G **35**, 104081 (2008).
[16] Chin-Hao Chen (PHENIX Collaboration), Hard Probes 2008 Intern. Conf. on Hard Probes of High Energy Nuclear Collisions, A Toxa, Galicia, Spain, 8–14 June 2008.
[17] E. Wenger (PHOBOS Collaboration), J. Phys. G **35**, 104080 (2008).
[18] M. J. Tannenbaum, Eur. Phys. J. C **61**, 747 (2009).
[19] Jiangyong Jia (PHENIX Collaboration), J. Phys. G **35**, 104033 (2008).
[20] M. van Leeuwen (STAR Collaboration), Eur. Phys. J. C **61**, 569 (2009).
[21] M. Daugherity (STAR Collaboration), J. Phys. G **35**, 104090 (2008).
[22] C. Y. Wong, Phys. Rev. C **76**, 054908 (2007).
[23] C. Y. Wong, Chin. Phys. Lett. **25**, 3936 (2008).
[24] C. Y. Wong, J. Phys. G **35**, 104085 (2008).
[25] C. Y. Wong, Phys. Rev. C **78**, 064905 (2008).
[26] C. Y. Wong, arXiv:0903.3879.
[27] E. Shuryak, Phys. Rev. C **76**, 047901 (2007).
[28] S. A. Voloshin, Nucl. Phys. **A749**, 287 (2005).
[29] C. B. Chiu and R. C. Hwa, Phys. Rev. C **79**, 034901 (2009).
[30] R. C. Hwa and C. B. Yang, Phys. Rev. C **67**, 034902 (2003); R. C. Hwa and Z. G. Tan, Phys. Rev. C **72**, 057902 (2005); R. C. Hwa and C. B. Yang, arXiv:nucl-th/0602024.
[31] C. B. Chiu and R. C. Hwa, Phys. Rev. C **72**, 034903 (2005).
[32] R. C. Hwa, arXiv:0708.1508.
[33] V. S. Pantuev, arXiv:0710.1882.
[34] A. Dumitru, F. Gelis, L. McLerran, and R. Venugopalan, Nucl. Phys. **A810**, 91 (2008).
[35] S. Gavin and G. Moschelli, J. Phys. G **35**, 104084 (2008).
[36] S. Gavin, L. McLerran, and G. Moschelli, Phys. Rev. C **79**, 051902 (2009).
[37] N. Armesto, C. A. Salgado, and U. A. Wiedemann, Phys. Rev. Lett. **93**, 242301 (2004).
[38] P. Romatschke, Phys. Rev. C **75**, 014901 (2007).
[39] A. Majumder, B. Muller, and S. A. Bass, Phys. Rev. Lett. **99**, 042301 (2007).
[40] A. Dumitru, Y. Nara, B. Schenke, and M. Strickland, Phys. Rev. C **78**, 024909 (2008); B. Schenke, A. Dumitru, Y. Nara, and M. Strickland, J. Phys. G **35**, 104109 (2008).
[41] R. Mizukawa, T. Hirano, M. Isse, Y. Nara, and A. Ohnishi, J. Phys. G **35**, 104083 (2008).
[42] Jianyong Jia and R. Lacey, Phys. Rev. C **79**, 011901 (2009).
[43] Jianyong Jia, Eur. Phys. J. C **62**, 255 (2009).
[44] O. Kaczmarek and F. Zantow, Phys. Rev. D **71**, 114510 (2005).
[45] C. Y. Wong, Phys. Rev. C **65**, 034902 (2002); **65**, 014903 (2002);

C. Y. Wong, J. Phys. G **28**, 2349 (2001); C. Y. Wong, Phys. Rev. C **72**, 034906 (2005); C. Y. Wong, talk presented at Recontre de Blois, Chateau de Blois, France, 15–20 May 2005, arXiv:hep-ph/0509088; C. Y. Wong, Phys. Rev. C **76**, 014902 (2007); C. Y. Wong, J. Phys. G **32**, S301 (2006).
[46] A. Schiz *et al.*, Phys. Rev. D **24**, 26 (1981).
[47] T. T. Chou and C. N. Yang, Phys. Rev. **170**, 1591 (1968).
[48] A. Bialas *et al.*, Acta Phys. Pol. B **8**, 855 (1977).
[49] E. M. Levin and Shekhter, in Proceedings of the IXth Winter LNPI School on Nuclear Physics and Elementary Particles, Leningrad, 1974.
[50] P. V. Landshoff and O. Nachtmann, Zet. Phys. C **35**, 405 (1988).
[51] O. Nachtmann, Ann. Phys. (NY) **209**, 436 (1991).
[52] H. G. Dosch, Phys. Lett. **B190**, 177 (1987); H. G. Dosch and Yu. A. Simonov, *ibid.* **B205**, 339 (1988); Yu. A. Simonov, Nucl. Phys. **B307**, 512 (1988).
[53] A. Krämer and H. G. Dosch, Phys. Lett. **B252**, 669 (1990).
[54] H. G. Dosch, E. Ferreira, and A. Krämer, Phys. Rev. D **50**, 1992 (1992).
[55] H. G. Dosch, O. Nachtmann, T. Paulus, and S. Weinstock, Eur. Phys. J. C **21**, 339 (2001).
[56] E. R. Berger and O. Nachtmann, Eur. Phys. J. C **7**, 459 (1999).
[57] A. DiGiacomo and H. Panagopoulos, Phys. Lett. **B285**, 133 (1992); A. DiGiacomo, H. Panagopoulos, and E. Meggiolaro, *ibid.* **B285**, 133 (1992).
[58] E. Meggiolaro, Phys. Lett. **B451**, 414 (1999).
[59] J. R. Forshaw and D. A. Ross, *Quantum Chromodynamics and the Pomeron* (Cambridge University Press, New York, 1997).
[60] S. Donnachie, G. Dosch, P. V. Landshoff, and O. Nachtmann, *Pomeron and QCD* (Cambridge University Press, New York, 2002).
[61] A. Casher, J. Kogut, and L. Susskind, Phys. Rev. D **10**, 732 (1974).
[62] J. D. Bjorken, Phys. Rev. D **27**, 140 (1983).
[63] C. Y. Wong, R. C. Wang, and C. C. Shih, Phys. Rev. D **44**, 257 (1991).
[64] C. Y. Wong, *Introduction to High-Energy Heavy-Ion Collisions* (World Scientific, Singapore, 1994).
[65] S. Wolfram, in Proceedings of the 15th Recontre de Moriond (1980), edited by Tran Thanh Van; G. C. Fox and S. Wolfram, Nucl. Phys. **B168**, 285 (1980); B. R. Webber, Nucl. Phys. **B238**, 492 (1984).
[66] L. Van Hove and A. Giovannini, Acta Phys. Pol. B **19**, 931 (1988); M. Garetto, A. Giovannini, T. Sjostrand, and L. van Hove, CERN Report CERN-TH-5252/88, presented at Perugia Workshop on Multiparticle Dynamics, Perugia, Italy, 21–28 June 1988; Y. L. Dokshizer, V. A. Khoze, and S. I. Troyan, in *Perturbative Quantum Chromodynamics*, edited by A. H. Mueller (World Scientific, Singapore, 1989), p. 241.
[67] R. O'dorico, Nucl. Phys. **B172**, 157 (1980); R. O'dorico, Comput. Phys. Commun. **32**, 139 (1984).
[68] B. Andersson, G. Gustafson, and T. Sjöstrand, Zeit. für Phys. C **20**, 317 (1983); B. Andersson, G. Gustafson, G. Ingelman, and T. Sjöstrand, Phys. Rep. **97**, 31 (1983); T. Sjöstrand and M. Bengtsson, Comput. Phys. Commun. **43**, 367 (1987); B. Andersson, G. Gustavson, and B. Nilsson-Alqvist, Nucl. Phys. **B281**, 289 (1987).
[69] A. Capella and A. Krzywicki, Phys. Rev. D **18**, 3357 (1978); A. Capella and J. Tran Thanh Van, Zeit. Phys. C **10**, 249 (1981); A. Capella *et al.*, *ibid.* **33**, 541 (1987); A. Capella and J. Tran Thanh Van, *ibid.* **38**, 177 (1988); N. Armesto and C. Pajares, Int. J. Mod. Phys. A **15**, 2019 (2000).
[70] K. Werner, Phys. Rev. D **39**, 780 (1989).
[71] H. Sorge, H. Stöcker, and W. Greiner, Nucl. Phys. **A498**, 567c (1989).
[72] C. Y. Wong and Z. D. Lu, Phys. Rev. D **39**, 2606 (1989).
[73] X. N. Wang and M. Gyulassy, Comput. Phys. Commun. **83**, 307 (1994).
[74] K. Geiger and B. Müller, Nucl. Phys. **A544**, 467c (1992).
[75] L. D. McLerran and R. Venugopalan, Phys. Rev. D **49**, 2233 (1994); **49**, 3352 (1994); **50**, 2225 (1994); A. Kovner, L. McLerran, and H. Weigert, *ibid.* **52**, 6231 (1995).
[76] Zi-Wei Lin, Che Ming Ko, Bao-An Li, Bin Zhang, and Subrata Pal, Phys. Rev. C **72**, 064901 (2005).
[77] S. Jeon and J. Kapusta, Phys. Rev. C **56**, 468 (1997).
[78] J. Schwinger, Phys. Rev. **128**, 2425 (1962); J. Schwinger, in *Theoretical Physics, Trieste Lectures*, 1962 (IAEA, Vienna, 1963), p. 89.
[79] J. H. Lowenstein and J. A. Swieca, Ann. Phys. (NY) **68**, 172 (1971).
[80] S. Coleman, R. Jackiw, and L. Susskind, Ann. Phys. **93**, 267 (1975).
[81] S. Coleman, Ann. Phys. **101**, 239 (1976).
[82] H. Aihara *et al.* (TPC/Two_Gamma Collaboration), Lawrence Berkeley Laboratory Report LBL-23737, 1988.
[83] W. Hofmann, Annu. Rev. Nucl. Sci. **38**, 279 (1988).
[84] A. Petersen *et al.* (Mark II Collaboration), Phys. Rev. D **37**, 1 (1988).
[85] K. Abe *et al.* (SLD Collaboration), Phys. Rev. D **59**, 052001 (1999).
[86] K. Abreu *et al.* (DELPHI Collaboration), Phys. Lett. **B459**, 397 (1999).
[87] Hongyan Yang (BRAHMS Collaboration), J. Phys. G **35**, 104129 (2008); K. Hagel (BRAHMS Collaboration), APS DNP 2008, Oakland, California, 23–27 October 2008.
[88] J. Casalderrey-Solana and C. A. Salgado, Acta Phys. Pol. B **38**, 3731 (2007); S. Wicks and M. Gyulassy, J. Phys. G **34**, S989 (2007); M. Gyulassy, P. Levai, and I. Vitev, Nucl. Phys. **B594**, 371 (2001); S. Wicks, S. Horowitz, W. Djordjevic, and M. Gyulassy, *ibid.* **A784**, 426 (2007); I. Vitev, Phys. Lett. **B639**, 38 (2006); E. Wang and X. N. Wang, Phys. Rev. Lett. **87**, 142301 (2001); E. Wang and X. N. Wang, *ibid.* **89**, 162301 (2002); A. Drees, H. Feng, and J. Y. Jia, Phys. Rev. C **71**, 034909 (2005); G. Wang and H. Huang, Phys. Lett. **B672**, 30 (2009).
[89] The author thanks Dr. Vince Cianciolo for suggesting the use of the near-side photon jet to distinguish different ridge models.
[90] T. Sjöstrand *et al.*, Comput. Phys. Commun. **135**, 238 (2001).
[91] Jiangyong Jia (PHENIX Collaboration), arXiv:0906.3776.
[92] F. E. Low, Phys. Rev. D **12**, 163 (1975); S. Nussinov, Phys. Rev. Lett. **34**, 1286 (1975).
[93] J. Dolejsi and J. Hufner, Z. Phys. C **54**, 489 (1992).
[94] Wei-Ning Zhang and C. Y. Wong, Phys. Rev. C **68**, 035211 (2003).
[95] M. A. Shifman, A. I. Vainshtein, and V. I. Akharov, Nucl. Phys. **B147**, 385 (1979); **B147**, 519 (1979).
[96] S. Narison, Nucl. Phys. Proc. Suppl. **54**, 238 (1997).
[97] R. J. Glauber, in *Lectures in Theoretical Physics*, edited by W. E. Brittin and L. G. Dunham (Wiley Interscience, New York, 1959), Vol. 1, p. 315.